From Local Interactions to Global Patterns: An Analysis of Silk Density in Spider Webs

Fangyuan Lin, Kathryn M. Nagel, Seewoo Lee, Jason Jiang,
Grant Yang, Patrtick Chang, Samuel Li, Norman Sheu

January 27, 2025

Abstract

This study explores the structural complexity of spider webs through information-theoretic and harmonicity-based frameworks to quantify spatial patterns in silk density across different web regions and reveal the underlying resource allocation strategies. By analyzing the entropy of silk density distributions across different species, we observed that the entropy values follow a normal distribution with a mean of 1.24 bits and a standard deviation of 0.22 bits when using 10 quantization levels. In the second part of the paper, by measuring the harmonicity of the silk density, we reveal that the silk density at a given point can be inferred from its neighbors, with an average harmonicity value of 0.0039 (fraction of total points in point cloud data). The harmonic behavior is notable for its maximum principle, suggesting that the strongest parts of the web appear at the boundaries, aligning with existing knowledge of spider web construction. These findings provide a new technique for quantifying web-building strategies and offer new insights into spider behavior and evolution.

1 Introduction

Spiders are exceptional biological engineers, using self-manufactured silk to design and build webs many times larger than their bodies [1]. As a material, spider silk is stronger and more elastic than almost any other known natural and man-made material, while simultaneously being biodegradable and biocompatible [2, 3, 4, 5]. Spiders use silk for a variety of purposes, including prey capture and wrapping, encasing egg sacks, and perhaps most visibly: building webs [6]. A spider's web serves as a tool for prey capture, an extension of the senses, and a retreat from predators [6, 7, 8, 9, 10]. Orb webs are the most ancient type of web, evolving more than 165 Mya, but many extant families abandoned orb webs later in their evolution [6, 11]. While some abandoned web building altogether, adopting a cursorial lifestyle, other families evolved web design of staggering variety.

The linyphioids group (Linyphiidae and Pimoidae) constitute about 10 percent of all spider species worldwide, with more than 4800 named species [12]. Despite linyphioid diversity and abundance, web architecture and mechanics are poorly studied. Linyphiids generally build clearly suspended horizontal sheet webs that are sparsely attached to the surrounding substrate; however, variations in this design are prevalent in most genera [12]. Sheet web structures are generally described as an unordered meshwork of silk fibers varying in thickness and strength, with some threads bearing viscid droplets [7, 13]. However, building a web is an energetically costly process, depleting glucoproteins and significantly increasing the metabolic rate [14, 15]. It is expected that over evolutionary time, selection would favor economical webs that maximize function with the least amount of silk [16, 17]. However, quantifying the effectiveness and economy of webs is a difficult process with no universally accepted metric, although mathematical

modeling has precedence for cob and orb web species [18, 19, 20, 21]. In order to quantify web complexity, we estimate the Shannon entropy and harmonicity of 3D scans of completed sheet webs. For a deeper explanation of Shannon entropy, harmonicity, and their significance to analyzing the structure of sheet webs, see Section 2.

To understand the process of web construction, scanned images are stacked to form a 3D model of the web work [18]. This process has been used to determine the purpose and importance of different stages in web construction, discern discrete stages of web construction, and estimate the mechanical properties of silk under stress in orb and tangle web species [22]. Namazi used the fractal dimension and Shannon entropy to quantify the complexity and information content of orb weaving spiders to correlate cognitive function with web structure by interpreting the brightness level of digitized images [23]. However, it is important to note that a spider web, being a continuous structure, theoretically has infinite information content. In this paper, we adopt a similar scanning and analysis approach, but focus on the entropy of the quantized silk density rather than the pixel brightness.

Another important aspect in spider web complexity is the spatial correlations in silk density [21]. By examining how the density of silk in one region of the web relates to the density in neighboring regions, we can infer patterns and predict the distribution of silk throughout the web. Understanding how silk densities vary across the 3D surface of a sheet web can potentially provide further insight into spider web building behavior and identify areas of the web used for different purposes, for example, prey capture compared to predator retreat [6, 12]. Furthermore, we measure how closely the silk density distribution across webs follows the mean value property. If a function satisfies the mean value property, the value the function takes at a point is equal to the average of the values of its neighbors. Functions that satisfy the mean value property are *harmonic functions*, which exhibit a range of notable properties. In particular, harmonic functions obey the maximum principle, which states that the highest values of the function appear at its boundary, an observed but typically unquantified trait of sheet webs [12, 1].

In this paper, we develop a method to quantify sheet web complexity by measuring Shannon entropy and harmonicity for the sheet webs of three species of linyphiid common to Northern California, *Neriene digna, Neriene litigiosa,* and *Microlinyphia dana.* Using these metric, we are able to discern new features of sheet webs and deepen our understanding of spider web-building behavior.

The remainder of the paper is organized as follows. In Sections 2 and 3, we provide background on the mathematical principles and experimental methodology respectively. In Section 4, we introduce and discuss the mathematical framework for quantifying the entropy of silk density distributions. Section 5 discusses the harmonicity of silk density and the analysis of local spatial correlations across the webs by modeling the silk density as a spatial stochastic process. Finally, Section 6 concludes the paper and suggests directions for future research.

2 What are Entropy and Harmonicity, and what do these values tell us about spider webs?

In this section, we give mathematical definitions of entropy and harmonicity, and explain how these concepts can be used to analyze silk density distribution of spider webs.

2.1 Mathematical Framework for Entropy Computation

Generally, Shannon entropy measures the amount of information needed to describe the spread of data across all possible values [24]. By examining the silk density distribution across a web, we can assign an entropy value to each web. A low entropy value would indicate that the silk density across the web is primarily concentrated at one value, while a high entropy value would indicate a web with a full range

of density values spread uniformly at random. The lowest possible entropy value is zero bit, and the highest is $\log_2(10) \approx 3.3219$ bits when quantizing with 10 density levels.

We develop a mathematical framework for computing the entropy of silk density distributions. The silk density distribution of a web can be determined by subdividing the three-dimensional space where the web is constructed by a cubic grid and then quantizing the silk density measurements into discrete levels. Crucially, this framework demonstrates a convergence property: as we refine the subdivisions of the spatial domain, the resulting entropy becomes asymptotically independent of how the region is subdivided.

Following Shannon's definition of entropy, we compute entropy of the density of a web as follows: Divide the whole box into $N = N_h \times N_w \times N_d$ smaller boxes of size $\frac{h}{N_h} \times \frac{w}{N_w} \times \frac{d}{N_d}$. For $0 \leqslant i < N_h, 0 \leqslant j < N_w, 0 \leqslant k < N_d$, let $n_{i,j,k}$ be the number of points in the corresponding small box $B_{i,j,k}$. Then the local density of a box is

$$\rho_{i,j,k} = \frac{n_{i,j,k}}{\#B_{i,j,k}} = \frac{n_{i,j,k}}{\frac{h}{N_h}\frac{w}{N_w}\frac{d}{N_d}}. \tag{1}$$

We group these densities into L different levels (bins), and compute the entropy of the corresponding distribution. To do this, we first compute ρ_{max}, the greatest density among all boxes. Then we subdivide the range from 0 to ρ_{max} into L equal intervals. Each density can then be categorized into its corresponding interval.

Definition 2.1 (Entropy of a web's silk density)**.** Define the *entropy* of a web W's silk density as

$$H(W; N_h, N_w, N_d, L) = -\sum_{1 \leqslant \ell \leqslant L} p_\ell \log p_\ell$$

where

$$p_\ell = \frac{\#\{(i,j,k) : \text{level}(\rho_{i,j,k}) = \ell\}}{N}$$

are the probability densities for each level $\ell \in \{1, 2, \ldots, L\}$.

To obtain a numerically stable entropy, densities with negligible local densities are filtered out. We set a threshold $\epsilon > 0$ and simply ignore the local densities $\rho_{i,j,k} < \epsilon$ (which we define as *level 0*).

Note that our definition of entropy depends on the choice of the subdivisions N_h, N_w, N_d and the number of levels L. However, we remark that in theory, the entropy converges as we take finer subdivisions.

Theorem 2.2 (Convergence of Silk Density Entropy with Respect to Subdivision)**.** *Assuming there exists a measurable underlying field of silk density over the box, as the subdivisions become finer (i.e., $N_h, N_w, N_d \to \infty$), the entropy $H(W; N_h, N_w, N_d, L)$ converges to a finite limit $H(W; L) \in \mathbb{R}_{\geqslant 0}$.*

For proofs and further remarks, see Supplementary Material.

The following figures present heat maps of the silk density distributions for two samples: one with a relatively low entropy value for the silk density distribution and the other with a relatively high entropy value.

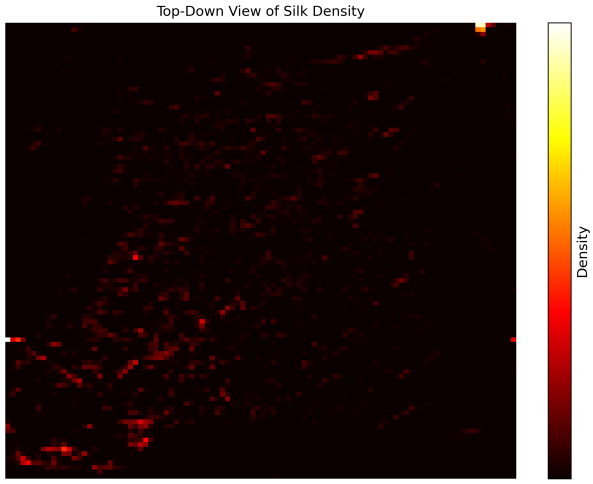

(a) Silk density distribution for a web sample exhibiting a relatively low entropy value (0.5589 bits), calculated by using 10 quantization levels and excluding the empty level. The web's structure displays consistently low silk density throughout. We remark that the majority of density levels correspond to the lowest level, reflecting energy-saving behavior. When subdividing the region 100 subdivisions on the length and width dimensions and 75 subdivision on the height dimension, the density level distribution is

$$[746096, 3520, 271, 78, 22, 6, 3, 2, 1, 1],$$

where the first entry represents the number of blocks with 0 density, the next entry represents the number of blocks with the lowest positive density level, and so on. This distribution indicates that most of the space is empty, with the lowest density level remaining dominant.

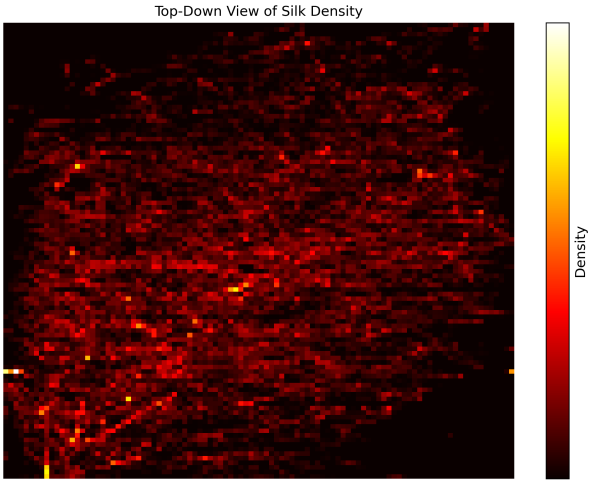

(b) Silk density distribution for a web sample exhibiting a relatively high entropy value (1.3300 bits), calculated by using 10 quantization levels and excluding the empty level. The spider employed a wider range of density levels throughout the structure, resulting in greater variation across the web. We remark that the majority of density levels are still the lowest level. When subdividing the region 100 subdivisions on the length and width dimensions and 75 subdivision on the height dimension, the density level distribution is

$$[737043, 8924, 2630, 951, 298, 111, 27, 11, 3, 2].$$

This distribution indicates that most of the space is still empty, with the lowest density level remaining relatively dominant.

It should be noted that, in theory, if the majority of the web has high silk density, the entropy would still remain low due to consistency. However, our observations indicate that as the spider invests more energy in adding silk to the web, the additional silk density is distributed in a relatively random manner. This randomness prevents the density levels from concentrating on specific values, thereby increasing the entropy as the spider enhances the web's density. Additionally, while high-density silk on the boundary provides structural integrity, the variability in silk density elsewhere reflects the spider's adaptive energy investment [25]. For example, varying silk densities can optimize the web for prey capture, as areas with lower density allow prey to escape more easily [1].

2.2 Mathematical Framework for Harmonicity

If you know your neighbors, do you know yourself? An important aspect in spider web complexity is the spatial correlations in silk density. By examining how the density of silk in one region of the web relates to the density in neighboring regions, we can infer patterns and predict the distribution of silk

throughout the web. In particular, we want to infer a silk density of a box based on densities of its neighboring boxes. The simplest way to do this is by taking the average density of the neighboring regions, which leads us to the concept of *harmonic functions*.

Let f be a function on a lattice $\mathbf{Z}^3$, the set of integer triples. We call f *harmonic* if the value of f at a point is equal to the average of f over neighboring points:

Definition 2.3 (Harmonic functions)**.** A function $f : \mathbf{Z}^3 \to \mathbf{R}$ is *harmonic* if $f(\mathbf{x})$ is equal to

$$\tilde{f}(\mathbf{x}) := \frac{1}{6} \sum_{\mathbf{y}:\|\mathbf{y}-\mathbf{x}\|_1=1} f(\mathbf{y})$$

for any $\mathbf{x} \in \mathbf{Z}^3$.

Equivalently, f is harmonic if and only if the *discrete Laplacian* Δf vanishes identically [26, 27]:

Definition 2.4 (Laplacian and Harmonicity)**.** For a function $f : \mathbf{Z}^3 \to \mathbf{R}$, the *Laplacian* of f is a function $\Delta f : \mathbf{Z}^3 \to \mathbf{R}$ defined as

$$\Delta f(\mathbf{x}) = \sum_{\mathbf{y}:\|\mathbf{y}-\mathbf{x}\|_1=1} (f(\mathbf{x}) - f(\mathbf{y})) \quad \forall \mathbf{x} \in \mathbf{Z}^3.$$

Harmoncity of f is defined as an L^2-norm of Δf.

There are some properties of (discrete) harmonic functions of our interests. For example, by definition, the value of a harmonic function at a point is determined as the average of the values of its neighbors. Also, they satisfy the *maximum principle*: any harmonic function should attain their minimum/maximum on boundaries of the domain.

As we mentioned above, we are interested in the spatial correlations in silk density. In particular, we want to infer a silk density of a box based on densities of its neighboring boxes. The simplest way to do this is by taking average of neighbor densities, and this would work perfectly if and only if the silk density function ρ is *harmonic*. By our earlier discussion, $\Delta\rho$ will be identically zero if and only if $\tilde{\rho} = \rho$. However, there is no reason for ρ to be a harmonic function a priori. Instead, we can use a generalized version of averages, and we consider *power means* as better alternatives. More precisely, we consider

$$\tilde{\rho}^{(\alpha)}_{i,j,k} := \left(\frac{1}{6} \sum_{\|(i',j',k')-(i,j,k)\|_1=1} \rho^{\alpha}_{i',j',k'} \right)^{1/\alpha}$$

and see if we get a better inference results for some $\alpha \geqslant 0$ other than $\alpha = 1$, which corresponds to the usual mean. The α-power mean would give a zero error if and only if ρ^α is harmonic. This let us to define α-harmonicity of silk density:

Definition 2.5 (α-harmonicity of silk density)**.** Define the *α-harmonicity* of a web W's silk density ρ as $\|\Delta(\rho^\alpha)\|_2$, the harmonicity of ρ^α.

We simply call 1-harmonicity as harmonicity. As entropy, α-harmonicity depends on the choice of subdivisions N and the number of levels L. Under mild hypothesis, we can show that there always exists best $\alpha = \alpha_* \in [0, \infty)$ that minimizes the α-harmonicity:

Theorem 2.6. *(Existence of the best α) Under mild hypothesis, for any spider web, there exists finite $\alpha = \alpha_* \geqslant 0$ where α-harmonicity of silk density ρ is minimized.*

See Theorem 7.4 in Supplementary Materials for details.

3 Methodology

3.1 Specimen Collection and Web Construction

Collected spiders were kept in small containers for 1-2 weeks without food prior to introduction to experimental space to ensure relative uniformity of physiological state. Specimens were placed inside 10.16 x 10.16 x 10.16 cm (4" x 4" x 4") acrylic boxes with clear sides, a black base, and no lid. Vaseline was coated on the inside top 2.54 cm (1")of each side to prevent specimens from escaping. Each spider was given 1-2 weeks in ambient conditions to complete a web. Linyphiids construct webs over the course of multiple days and weeks, and web completion was defined as the point at which no additional silk was added to the web after several consecutive days [28].

3.2 Web Scanning

Completed webs were placed into an enclosed experimental scanning apparatus blocking all outside light. Scanning was conducted by a laser (Quarton Inc. VLM-520-56) and camera (Canon EOS R5C mirrorless camera using a Canon RF 100mm F 2.8 Macro lens) mounted on a track at a fixed distance (0.67 meter). A small motor (Habow Technic Power-Functions XL-Motor-Set 8882) was used to advance the laser and camera simultaneously to scan the length of the experimental chamber from front to back, recording at 120 FPS for 20-30 seconds. An infrared laser distance sensor (DFROBOT DFRduin Uno v3.0[R3]) monitored the location of the camera relative to its start position to provide z-axis information for 3D reconstruction.

3.3 Data Processing and Extraction

Individual video frames representing two dimensional slices of the web were extracted for cleaning and analysis using a custom Python script [29]. For each video, a set cropped region was identified in each frame that excluded the box edges and background and accounted for any minute changes in elevation across the length of the box. Red and blue color values were reset to the minimum value and the image converted to grayscale. Background noise was removed using a minimum threshold filter of 0.55 max RGB value. Three-dimensional Point Cloud Data (PCD) representations of each web were created using the filtered data. Examples of the three-dimensional PCD plots are shown in Figure 2.

3.4 Quantification of Silk Density

We approximate the silk density in a region by counting the number of coordinate points in that region of the corresponding Point Cloud Data document, divided by volume of that region. The historical method to determine silk density would be to physically cut each web over a partition and then measure the silk mass for each subdivision [30]. However, this approach poses practical challenges and destroys the web in the process. Using PCD representations yields us to gather accurate data while maintaining the web for further scanning or experimentation.

3.5 Statistical Analysis

Four data points representing entropy and harmonicity values for each web were analyzed in R 4.3 (http://R-project.org/): h (entropy), h0 (entropy computed by excluding the zero-density-level), global harmonicity, and α_*. Data exploration and analysis followed [31]. Outliers were removed based on IQR quartiles and data was tested for normality using Krusal-Wallis tests and Levene's test for homogeneity of variance. The influence of discrete factors (species, genus, SampleID, sex, and age) were analyzed using ANOVAs models. ANOVA tests for call combinations of categorical variables were also performed,

as well as multiple linear regression models that combined all variables. Comparisons between models were made using Tukey's HSD.

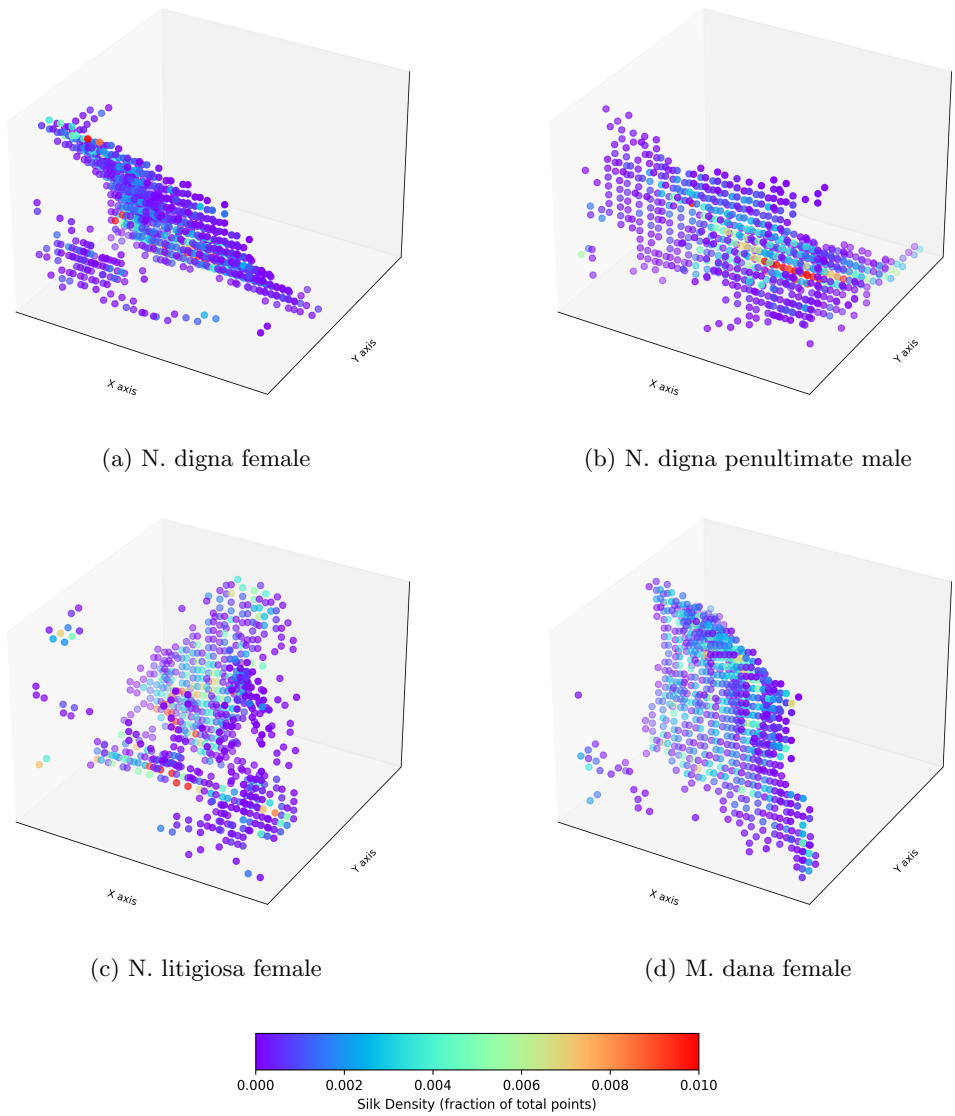

(a) N. digna female

(b) N. digna penultimate male

(c) N. litigiosa female

(d) M. dana female

Figure 2: Visual representations of the silk density plots for four sheet webs from the three experimental species. These visualizations are derived from the PCD representation of the spider webs. The density in each region is computed based on the fraction of points within that region, relative to the total number of points. Purple colors represent less dense (or more sparse) areas of silk, while red areas indicate higher silk density.

4 Entropy of the Silk Density Results and Discussion

In this section, we address the question: *Is the silk density of a web consistent across its structure?* Our analysis reveals that the silk density exhibits a high degree of consistency, as indicated by the low entropy of the density level distribution - the average of the entropy across the samples consistently converges to approximately 0.083 bits (including the zero-density-level) and 1.24 bits (excluding zero-density-level) with respect to the number of samples for the spider species analyzed in this study, when using 10 quantization levels (Table 1). To reduce sensitivity to the choice of subdivision size, we apply a moving average approach to the subdivision parameters. Specifically, the subdivisions are varied from 100 to 120 along the length and width dimensions, and from 75 to 100 along the height dimension. No significant effects of species, genus, SampleID, sex, and age were identified; however, entropy values for the three experimental species are included in Figure 3. One might wonder whether using more quantization levels than 10 could capture additional information about the silk density distribution. However, we tested the computation with up to 100 quantization levels, and the resulting box plot yielded a shape similar to that obtained with 10 levels. Increasing the number of density levels does not significantly alter the results under the current experimental conditions. The entropy value (h0, excluding zero-density-level) is 73 percent lower than the theoretical maximum of $\log_2 10 \approx 3.32$, reflecting an uneven distribution of density levels.

The majority of the silk density falls within the lowest quantization level, suggesting an energy-saving behavior by the spiders. This low entropy reflects a strong bias toward minimal silk usage, possibly prioritizing efficiency of resource use [15, 14, 32]. The production of silk and the construction of a web are energy intensive processes and are directly influenced by the physiological state of the spider and a number of ecological factors [6]. Among linyphiids species, silk density can range from quite sparse, as seen in *Laminacauda ansoni* to very dense in *Pocobletus versicolor*, where distinguishing individual thread lines is difficult [12]. Our results indicate that the sheet web spiders tested may optimize the amount of silk needed for effective prey capture while conserving energy. The low density could also be a factor of starvation, as some orb web spiders change the size and density of webs based during periods of starvation and on prey availability [6].

Alternatively, a relatively higher entropy would imply a more uniform use of different density levels, which could indicate that the spider may prioritize different factors of web performance across neighboring web sections related to varying functional purposes. For example, a dense region necessary for structural support adjacent to a sparse region of sticky silk for prey capture. This was not observed in the species used in this paper, and integrating greater diversity into future studies will either support low entropy as a universal feature of sheet webs or reject this conclusion and illuminate environmental and behavioral traits linked with differing entropy levels.

Species	**n**	**h in bits**	**h (excl. level 0) in bits**
N. digna	23	0.0797	1.18
N. litigiosa	5	0.0854	1.33
M. dana	13	0.0864	1.31

Table 1: Calculated entropy values by species. Two values for entropy are shown, the first (h) integrating all sections of the scanned area including empty space (level 0). The second (h excl. level 0) removes empty space (level 0). Excluding level 0 allows us to compare the density levels only where silk is present, and more accurately reflects the organization of the sheet web.

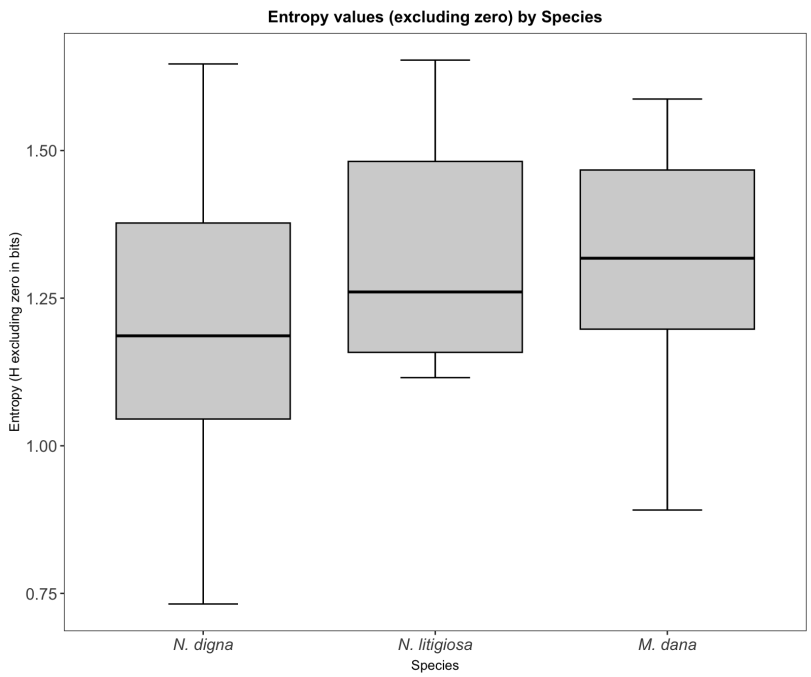

Figure 3: Entropy values (excl. level zero) in bits for three linyphiid species. We use 10 density levels for calculating the entropy. No signifcant differences were found between the three species tested, *N. digna, N. ligitiosa,* and *M. dana*.

5 Harmonicity Results and Discussion

In this section, we address the question: *Can we infer silk density of a web by neighbors?* Using the mathematical framework described in Section 2.2, we calculated the global harmonicity of silk density ($\|\Delta\|_2$). No significant effects of species, genus, sex, and age were identified, and results include data from all trials once outliers were removed. For all webs, the average harmonicity value was 0.0039 (fraction of total points in PCD, Table 2): harmonicity for the three linyphiid species are included in Figure 4 (left). The harmonic behavior displayed in the silk density indicates that the silk is lain at similar densities across the surface of the sheet web, even when the specific shape of the web varies.

Also, we measure the α-harmonicity of each web and found the best $\alpha = \alpha_*$ that minimizes the error, as mentioned at the end of Section 2.2 (see also Theorem 2.6). We compute the harmonicity of ρ^α by varying the α value in increments of 0.01 and find the $\alpha = \alpha_*$ that minimizes $\|\Delta(\rho^\alpha)\|_2$. We found that the average α_* is consistent over species, genus, sex, and age, at 0.95 (Table 2). In other words, $(\text{silk density})^{0.95}$ is approximately harmonic. α_* for the three linyphiid species are included in Figure 4 (right).

Species	**n**	Mean $\|\Delta\|_2$	α_*
N. digna	23	0.00360	0.951
N. litigiosa	5	0.00496	0.942
M. dana	13	0.00398	0.938

Table 2: Harmonicity and α_* for web scans separated by species. We use 20 subdivisions on the length and width dimensions and 15 subdivision on the height dimension. No significant differences were found between the species studied.

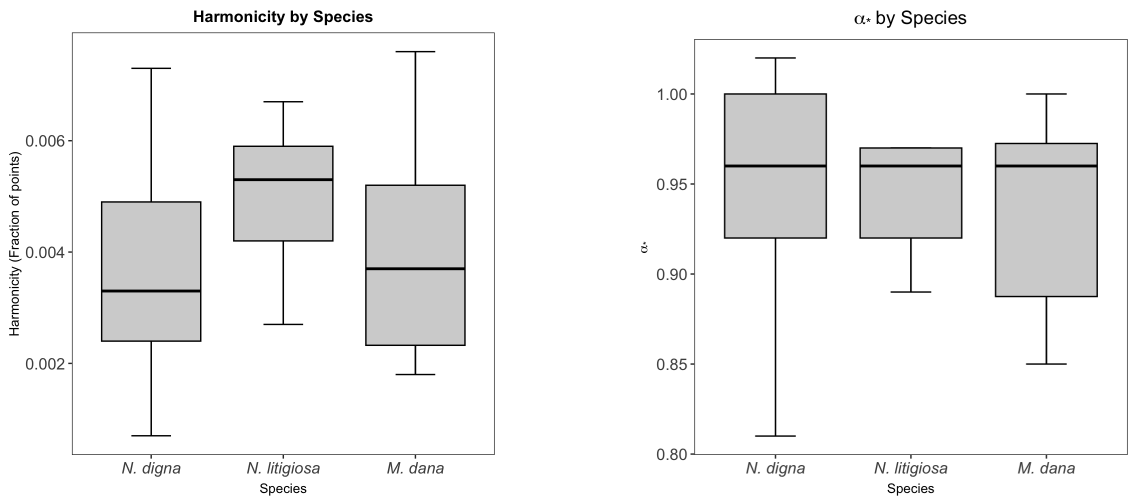

Figure 4: Harmonicity and α_* for linyphiid species. No signifcant differences were found between the three species tested, *N. digna, N. ligitiosa,* and *M. dana*.

6 Conclusions

In three species of linyphiid spiders, completed sheet-webs exhibit traits consistent with organization, optimization, and harmonicity, despite appearing random to the human eye. While the specifics of the organization and design are not yet known, the low entropy values provide evidence that the "unordered meshwork" is rather a deliberate network of silk fiber [7].

We found the entropy and harmonicity values did not differ between the three species tested (*N. digna, N. litigiosa,* and *M. dana*). This indicates that these sheet web properties measured are conserved across the closely related genera, and that having a harmonic web with low entropy may provide some fitness benefit. Identifying conserved traits may provide insight into the critical features of an effective sheet-web, and this knowledge can be applied to engineering and architectural design [9]. However, these measures do not account for several other important features of web design that are known to impact prey capture effectiveness, such as shape, use of different silks, and size [7, 33, 6]. Further experimentation integrating these additional qualities and species from globally distributed genera is needed to completely describe linyphiid webs.

This study had several limitations. First, the type and physical properties of the silk across different parts of the web were not measured. Linyphiids create webs using a variety of fibers generated from different combinations of silk glands. Silk fibers vary greatly in thickness, protein structure, and some contain sticky globules thought to aid in prey capture [7]. Each of these factors likely influence the structure and design of sheet webs, and should be included in future studies as we develop more advanced scanning

and analysis techniques [7]. Web construction was also confined to a 10.16 x 10.16 x 10.16 cm box, although this restriction is necessary for direct comparison between individuals. The number of species used was also limited, and all three species used co-occur in a small area, indicating overlapping niche space. Expanding this analysis to species outside this narrow niche would help determine how conserved the design of sheet-webs are across the Linyphiid family and identify factors unique to webs adapted to different environmental conditions [12]. Including species from each sub-family within Linyphiidae could provide insight into the evolution and diversification of this understudied group [33].

Moving forward, we can use these imaging and quantification methods to investigate web design in a wide variety of spider species across different environmental conditions and stressors. While only completed webs were scanned in this study, this non-destructive approach will allow us to obtain 3D scans of webs across every stage of construction, providing further insight into the step-by-step process used to create a viable sheet-web. The 3D web scans can be analyzed in more detail to discern additional physical and geometric properties, and may be used to inform computational models of sheet-webs.

From a microscopic perspective, metrics such as clustering coefficients, degree distributions, and modularity can be computed to analyze the graph structure of sheet webs. Viewing sheet webs as complex networks can provide deeper insights towards the specifics of thread organization and how this contributes towards the functionality of the web as both a shelter and a prey trap [34]. From a macroscopic perspective, efforts are already underway to derive equations that can accurately model the surfaces of the webs have already scanned. With these equations, we will investigate whether sheet webs exhibit characteristics of minimal surfaces. We can also simulate these webs with such equations to test the viability of using webs as a model for applications in electronics and material science. With a sufficiently large dataset of spider web scans, machine learning models can be trained to generate web-like structures with similar properties.

Understanding the physical properties of sheet webs may also provide inspiration for engineering and architectural designs that minimize material usage while maintaining structural function. Identifying the unseen patterns of nature is a powerful tool, and the non-destructive scanning technique and quantification of entropy and harmonicity described here have the potential to illuminate many undiscovered nuances in the structure and design of spider webs.

Ethics

This work did not require ethical approval from a human subject or animal welfare committee.

Author Contributions

Conceptualization: S. Lee, F. Lin, N. Sheu; Data Curation: P. Chang, J. Jiang, S. Lee, S. Li, F. Lin, K. Nagel, N. Sheu, G. Yang; Investigation: P. Chang, J. Jiang, S. Lee, S. Li, F. Lin, K. Nagel, N. Sheu, G. Yang; Methodology: J. Jiang, S. Lee, F. Lin, K. Nagel, N. Sheu, G. Yang; Software: P. Chang, J. Jiang, S. Lee, S. Li, F. Lin, K. Nagel, G. Yang; Formal analysis: J. Jiang, S. Lee, F. Lin, K. Nagel, N. Sheu, G. Yang; Validation: J. Jiang, S. Lee, F. Lin, K. Nagel, N. Sheu, G. Yang; Visualization: J. Jiang, S. Lee, F. Lin, K. Nagel, G. Yang; Writing-original draft: J. Jiang, S. Lee, F. Lin, K. Nagel, N. Sheu, G. Yang; Writing-review and editing: J. Jiang, S. Lee, F. Lin, K. Nagel, N. Sheu; Resources: J. Jiang, S. Lee, F. Lin, K. Nagel, N. Sheu, G. Yang; Supervision: F. Lin, N. Sheu; Project Administration: N. Sheu. All authors have read and agreed to the published version of the manuscript.

Conflict of Interest Declaration

We declare we have no competing interests.

Funding

This research did not receive external funding.

References

[1] Foelix R. Biology of spiders. Oxford university press; 2010.

[2] Römer L, Scheibel T. The elaborate structure of spider silk: structure and function of a natural high performance fiber. Prion. 2008;2(4):154-61.

[3] Ko FK, Wan LY. Engineering properties of spider silk. Handbook of properties of textile and technical fibres. 2018:185-220.

[4] Lewis RV. Spider silk: the unraveling of a mystery. Accounts of chemical research. 1992;25(9):392-8.

[5] Harmer AM, Blackledge TA, Madin JS, Herberstein ME. High-performance spider webs: integrating biomechanics, ecology and behaviour. Journal of the Royal Society Interface. 2011;8(57):457-71.

[6] Blackledge TA, Kuntner M, Agnarsson I. The form and function of spider orb webs: evolution from silk to ecosystems. In: Advances in insect physiology. vol. 41. Elsevier; 2011. p. 175-262.

[7] Benjamin SP, Düggelin M, Zschokke S. Fine structure of sheet-webs of Linyphia triangularis (Clerck) and Microlinyphia pusilla (Sundevall), with remarks on the presence of viscid silk. Acta Zoologica. 2002;83(1):49-59.

[8] Lott M, Poggetto VFD, Greco G, Pugno NM, Bosia F. Prey localization in spider orb webs using modal vibration analysis. Scientific Reports. 2022;12(1):19045.

[9] Hill PS, Lakes-Harlan R, Mazzoni V, Narins PM, Virant-Doberlet M, Wessel A, et al. Biotremology: studying vibrational behavior. vol. 6. Springer; 2019.

[10] Mortimer B. A spider's vibration landscape: adaptations to promote vibrational information transfer in orb webs. Integrative and Comparative Biology. 2019;59(6):1636-45.

[11] Dimitrov D, Lopardo L, Giribet G, Arnedo MA, Álvarez-Padilla F, Hormiga G. Tangled in a sparse spider web: single origin of orb weavers and their spinning work unravelled by denser taxonomic sampling. Proceedings of the Royal Society B: Biological Sciences. 2012;279(1732):1341-50.

[12] Hormiga G, Eberhard WG. Sheet webs of linyphioid spiders (araneae: linyphiidae, pimoidae): the light of diversity hidden under a linguistic basket. Bulletin of the Museum of Comparative Zoology. 2023;163(8):279-415.

[13] Peters HM, Kovoor J. The silk-producing system of Linyphia triangularis (Araneae, Linyphiidae) and some comparisons with Araneidae: structure, histochemistry and function. Zoomorphology. 1991;111:1-17.

[14] Schmitz A. Respiration in spiders (Araneae). Journal of Comparative Physiology B. 2016;186:403-15.

[15] Peakall DB, Witt PN. The energy budget of an orb web-building spider. Comp Biochem Physiol A. 1976;54(1976):187-90.

[16] Brown JH, Gillooly JF, Allen AP, Savage VM, West GB. Toward a metabolic theory of ecology. Ecology. 2004;85(7):1771-89.

[17] Brown JH, Burger JR, Hou C, Hall CA. The pace of life: metabolic energy, biological time, and life history. Integrative and Comparative Biology. 2022;62(5):1479-91.

[18] Su I, Narayanan N, Logrono MA, Guo K, Bisshop A, Mühlethaler R, et al. In situ three-dimensional spider web construction and mechanics. Proceedings of the National Academy of Sciences. 2021;118(33):e2101296118.

[19] Herberstein ME, Tso IM. Evaluation of formulae to estimate the capture area and mesh height of orb webs (Araneoidea, Araneae). The Journal of Arachnology. 2000;28(2):180-4.

[20] Corver A, Wilkerson N, Miller J, Gordus A. Distinct movement patterns generate stages of spider web building. Current Biology. 2021;31(22):4983-97.

[21] Venter C, Haddad CR, Codron D. A novel approach to determine the surface area of buckspoor spider webs and other irregular-shaped two-dimensional objects. MethodsX. 2022;9:101904.

[22] Su I, Buehler MJ. Mesomechanics of a three-dimensional spider web. Journal of the Mechanics and Physics of Solids. 2020;144:104096.

[23] Namazi HR. The complexity based analysis of the correlation between spider's brain signal and web. ARC Journal of Neuroscience. 2017;2(3):34-44.

[24] Shannon CE. A mathematical theory of communication. The Bell system technical journal. 1948;27(3):379-423.

[25] Tanaka K. Energetic cost of web construction and its effect on web relocation in the web-building spider Agelena limbata. Oecologia. 1989;81:459-64.

[26] Duffin R. Basic properties of discrete analytic functions. Duke Math J. 1956;23(1):335-63.

[27] Benjamini I, Lovász L. Harmonic and analytic functions on graphs. Journal of Geometry. 2003;76:3-15.

[28] Benjamin SP, Zschokke S. Homology, behaviour and spider webs: web construction behaviour of Linyphia hortensis and L. triangularis (Araneae: Linyphiidae) and its evolutionary significance. Journal of Evolutionary Biology. 2004;17(1):120-30.

[29] Lab G. `spiderweb`; 2025. [Online; accessed 26-Jan-2025]. `https://github.com/normansheu/spiderweb`.

[30] Sensenig A, Agnarsson I, Blackledge T. Adult spiders use tougher silk: Ontogenetic changes in web architecture and silk biomechanics in the orb-weaver spider. Journal of Zoology. 2011;285(1):28-38.

[31] Zuur AF, Ieno EN, Elphick CS. A protocol for data exploration to avoid common statistical problems. Methods in ecology and evolution. 2010;1(1):3-14.

[32] Kawamoto TH, Machado FdA, Kaneto GE, Japyassu HF. Resting metabolic rates of two orbweb spiders: A first approach to evolutionary success of ecribellate spiders. Journal of Insect Physiology. 2011;57(3):427-32.

[33] Arnedo MA, Hormiga G, Scharff N. Higher-level phylogenetics of linyphiid spiders (Araneae, Linyphiidae) based on morphological and molecular evidence. Cladistics. 2009;25(3):231-62.

[34] Manoj B, Chakraborty A, Singh R. Complex networks: A networking and signal processing perspective; 2018.

[35] Cover T, Thomas JA. Elements of information theory. Hoboken, NJ: Wiley-Interscience; 2006.

7 Supplementary Material

7.1 Proof of Theorem 2.2

Proof. We aim to show that the empirical distribution $\hat{P}_N$ of the quantized silk densities converges in total variation distance (i.e. L_1 distance) to the true distribution P as the number of subdivisions $N \to \infty$, and consequently, the entropy $H(W; N_h, N_w, N_d, L)$ converges to $H(W; L)$.

Let $D \subset \mathbb{R}^3$ be the spatial domain of the spider web with total volume V. We partition D into $N = N_h N_w N_d$ small boxes $\{B_i\}_{i=1}^N$ of equal volume $\delta V = \frac{V}{N}$.

For each box B_i, define:

- $\rho_i := \frac{1}{\delta V} \int_{B_i} \rho(\mathbf{x})\, d\mathbf{x}$, the average silk density in box B_i, where $\rho(\mathbf{x})$ is the silk density at point $\mathbf{x}$. By assumption, the silk density ρ exists and is a field (not necessarily continuous) that integrates to the silk mass.
- $X_i := \text{level}(\rho_i)$, the quantized silk density level assigned to ρ_i using L discrete silk levels.

Define the empirical distribution of silk density levels $\hat{P}_N$ over the levels $\{1, 2, \ldots, L\}$ as $\hat{p}_\ell := \frac{1}{N} \sum_{i=1}^N \mathbf{1}_{\{X_i = \ell\}}$, and the true probability distribution P of the silk density levels is $p_\ell = \frac{1}{V} \int_D \mathbf{1}_{\{\text{level}(\rho(\mathbf{x}))=\ell\}}\, d\mathbf{x}$.

Our goal is to show that:

$$\|\hat{P}_N - P\|_1 = \sum_{\ell=1}^{L} |\hat{p}_\ell - p_\ell| \to 0 \quad \text{as } N \to \infty.$$

1. Let ℓ be a silk density level. We consider the difference between $\hat{p}_\ell$ and p_ℓ:

$$\hat{p}_\ell - p_\ell = \frac{1}{N} \sum_{i=1}^{N} \mathbf{1}_{\{X_i=\ell\}} - \frac{1}{V} \int_D \mathbf{1}_{\{\text{level}(\rho(\mathbf{x}))=\ell\}}\, d\mathbf{x}.$$

   Rewrite $\hat{p}_\ell$ in terms of integrals over D:

$$\hat{p}_\ell = \frac{1}{N} \sum_{i=1}^{N} \mathbf{1}_{\{X_i=\ell\}} = \frac{1}{V} \sum_{i=1}^{N} \delta V \cdot \mathbf{1}_{\{\text{level}(\rho_i)=\ell\}} = \frac{1}{V} \sum_{i=1}^{N} \int_{B_i} \mathbf{1}_{\{\text{level}(\rho_i)=\ell\}}\, d\mathbf{x}.$$

   Therefore, the difference between the empirical probability of level ℓ and the true probability of level ℓ is then:

$$\hat{p}_\ell - p_\ell = \frac{1}{V} \sum_{i=1}^{N} \int_{B_i} \left[\mathbf{1}_{\{\text{level}(\rho_i)=\ell\}} - \mathbf{1}_{\{\text{level}(\rho(\mathbf{x}))=\ell\}}\right] d\mathbf{x}.$$

   By the triangle inequality, the absolute difference is:

$$|\hat{p}_\ell - p_\ell| \leqslant \frac{1}{V} \sum_{i=1}^{N} \int_{B_i} \left|\mathbf{1}_{\{\text{level}(\rho_i)=\ell\}} - \mathbf{1}_{\{\text{level}(\rho(\mathbf{x}))=\ell\}}\right| d\mathbf{x}.$$

   The integrand $\left|\mathbf{1}_{\{\text{level}(\rho_i)=\ell\}} - \mathbf{1}_{\{\text{level}(\rho(\mathbf{x}))=\ell\}}\right|$ is non-zero only when $\text{level}(\rho_i) \neq \text{level}(\rho(\mathbf{x}))$ within B_i.

2. By assumption, the silk density function $\rho(\mathbf{x})$ is measurable with respect to the Borel measure, as it is a physical property defined over the domain D. The quantization function $\text{level}(\cdot)$ maps real numbers to discrete levels based on fixed thresholds, making it a measurable function. Therefore, $\text{level}(\rho(\mathbf{x}))$ is measurable as the composition of measurable functions. The average density ρ_i is a constant on B_i (since ρ_i is the integral average over B_i), and thus measurable. Define the functions:

$$\phi_N(\mathbf{x}) = \mathbf{1}_{\{\text{level}(\rho_i)=\ell\}} \quad \text{for } \mathbf{x} \in B_i, \quad \phi(\mathbf{x}) = \mathbf{1}_{\{\text{level}(\rho(\mathbf{x}))=\ell\}} \quad \forall \mathbf{x} \in D,$$

which are measurable. Then:

$$|\hat{p}_\ell - p_\ell| \leqslant \frac{1}{V} \int_D |\phi_N(\mathbf{x}) - \phi(\mathbf{x})| \, d\mathbf{x}.$$

Since ρ_i is the average of $\rho(\mathbf{x})$ over $\mathbf{x} \in B_i$, i.e. $\rho_i = \frac{1}{\delta V} \int_{B_i} \rho(\mathbf{x}) \, d\mathbf{x}$, and $\delta V \to 0$ as $N \to \infty$ by assumption, by the *Lebesgue Differentiation Theorem*, for almost every $\mathbf{x} \in B_i$, $\lim_{\delta V \to 0} \rho_i = \rho(\mathbf{x})$.

3. Since $\rho_i \to \rho(\mathbf{x})$ as $N \to \infty$ almost everywhere in box D, a compact spatial region, and the quantization function level$(\cdot)$ is continuous except at finitely many thresholds $\{t_k\}$, for almost every $\mathbf{x} \in D$, level(ρ_i) = level$(\rho(\mathbf{x}))$ for N sufficiently large by uniform convergence. This implies that $\phi_N(\mathbf{x}) \to \phi(\mathbf{x})$ almost everywhere in D as $N \to \infty$.
4. Since $0 \leqslant |\phi_N(\mathbf{x}) - \phi(\mathbf{x})| \leqslant 1$, and D has finite measure V (our box has finite volume), apply the *Dominated Convergence Theorem* to conclude that:

$$\int_D |\phi_N(\mathbf{x}) - \phi(\mathbf{x})| \, d\mathbf{x} \to 0 \quad \text{as } N \to \infty.$$

Therefore:

$$|\hat{p}_\ell - p_\ell| \leqslant \frac{1}{V} \int_D |\phi_N(\mathbf{x}) - \phi(\mathbf{x})| \, d\mathbf{x} \to 0 \quad \text{as } N \to \infty.$$

Summing over all levels:

$$\|\hat{P}_N - P\|_1 = \sum_{\ell=1}^{L} |\hat{p}_\ell - p_\ell| \leqslant \frac{1}{V} \int_D \sum_{\ell=1}^{L} |\phi_N(\mathbf{x}) - \phi(\mathbf{x})| \, d\mathbf{x} \to 0 \quad \text{as } N \to \infty.$$

5. Finally, the entropy function $H(P) = -\sum_{\ell=1}^{L} p_\ell \log_2 p_\ell$ is continuous with respect to the variational distance. Since $\hat{P}_N \to P$ in variational distance, we have:

$$H(\hat{P}_N) \to H(P) \quad \text{as } N \to \infty.$$

□

Remark 7.1 (Importance of Finite Number of Levels)**.** Note that all Shannon's information measures are continuous (with respect to variational distance) when the alphabet of the random variable is finite [35]. For countably infinite alphabets, Shannon's information measures are actually everywhere discontinuous. Since the silk density is bounded over the box, quantization yields finitely many levels and the continuity of entropy over the probability measures on the silk density levels is thus guaranteed.

In practice, we use the maximal density sampled to categorize the densities into a fixed number of levels. In theory, the entropy value still converges since the maximum density sampled converges as we take finer and finer subdivisions. The following figure shows convergence for a particular web.

The following corollary remarks that the limiting entropy value as we take finer and finer subdivisions is independent of how the space is subdivided as long as the subdivisions become finer and finer.

Corollary 7.2. *Asymptotically, the entropy is independent of the way we sample the blocks as the number of subdivisions tends to ∞, as long as each volume of each subdivision tends to* 0.

Proof. In the proof above, the empirical distribution of quantized silk densities converges to the true distribution as the total number of subdivisions $N \to \infty$, without specifying the behavior of N_w, N_h and N_d. □

Now we discuss the choice of resolution, i.e. the number silk density levels :, in our quantization approach. With the fixed space-subdivision scheme (N_w, N_h, N_d), as $L \to \infty$ every bin would contain at most one data (density value) almost surely, which gives the maximum entropy of $\log n$. Note that the entropy is bounded by the constant that only depends on the total number of samples. In fact, we have the following inequality for the comparison of two entropy calculations, one with L levels and the other with mL levels:

Theorem 7.3. *Fix N_h, N_w, N_d and let $H(W; L) = H(W, N_h, N_d, N_w, L)$. For an integer $m \geqslant 1$, we have*

$$H(W; mL) \leqslant H(W; L) + \log m$$

Proof. Let n_ℓ (resp. n'_ℓ) be the number of samples (local densities) of level ℓ with maximum level L (resp. mL). Then we have $n_\ell = n'_{m\ell-(m-1)} + \cdots + n'_{m\ell}$ (the bin corresponds to the level ℓ is partitioned into m-bins with new levels $m\ell - (m-1), m\ell - (m-2), \ldots, m\ell$). By Jensen's inequality (applied to $f(x) = -x \log x$), we have

$$\begin{aligned} &-\frac{n_\ell}{mn} \log \frac{n_\ell}{mn} \geqslant \frac{1}{m} \sum_{0 \leqslant j < m} -\frac{n'_{m\ell-j}}{n} \log \frac{n'_{m\ell-j}}{n} \\ \Leftrightarrow &-\sum_{0 \leqslant j < m} \frac{n'_{m\ell-j}}{n} \log \frac{n'_{m\ell-j}}{n} \leqslant -\frac{n_\ell}{n} \log \frac{n_\ell}{n} + \frac{n_\ell}{n} \log m. \end{aligned}$$

Then we get

$$\begin{aligned} H(W; mL) &= \sum_{1 \leqslant \ell \leqslant mL} -\frac{n'_\ell}{n} \log \frac{n'_\ell}{n} = \sum_{1 \leqslant \ell \leqslant L} \sum_{0 \leqslant j < m} -\frac{n'_{m\ell-j}}{n} \log \frac{n'_{m\ell-j}}{n} \\ &\leqslant \sum_{1 \leqslant \ell \leqslant L} \left[-\frac{n_\ell}{n} \log \frac{n_\ell}{n} + \frac{n_\ell}{n} \log m \right] = H(W; L) + \log m. \end{aligned}$$

□

This theorem shows that increasing the number of silk density levels from L to mL increases the entropy by at most $\log m$.

7.2 Inference of Silk Density Using the α-Average of the Neighbors

For positive numbers $x_1, x_2, \ldots, x_n > 0$ and $\alpha > 0$, *α-power mean* is given by

$$M_\alpha(x_1, \ldots, x_n) := \left(\frac{1}{n} \sum_{i=1}^{n} x_i^\alpha \right)^{1/\alpha}.$$

Note that the limit of $\alpha \to 0^+$ approaches to the geometric mean $(x_1 \cdots x_n)^{1/n}$. Applying this to our situation, we can define α-averaged silk density $\tilde{\rho}^{(\alpha)}$ as

$$(\tilde{\rho}^{(\alpha)})_{i,j,k} := \left(\frac{1}{6} \sum_{\|(i',j',k')-(i,j,k)\|_1 = 1} \rho^\alpha_{i',j',k'} \right)^{1/\alpha}$$

and see which α works the best, by measuring the error between ρ and $\tilde{\rho}^{(\alpha)}$. Note that the error is zero, i.e., $\tilde{\rho}^{(\alpha)} \equiv \rho$, if and only if ρ^α is a harmonic function, and the maximum principle still applies to such density distribution ρ. We can show that, under technical assumptions, the silk density error attains minimum at some *finite* $\alpha_* \geqslant 0$.

Theorem 7.4. *For a web W with silk density ρ satisfying*

$$\sum_{(i,j,k)} \operatorname{sign}(\rho_{i,j,k} - \tilde{\rho}^{\infty}_{i,j,k}) \cdot \left(\frac{1}{6} \sum_{(i',j',k')} \rho^{\alpha}_{i',j',k'} \log \rho^{\alpha}_{i',j',k'} - \log \left(\frac{1}{6} \sum_{(i',j',k')} \rho^{\alpha}_{i',j',k'} \right) \right)^2 > 0, \tag{2}$$

there exists $0 \leqslant \alpha_* < \infty$ such that

$$\alpha_* = \operatorname{argmin}_{\alpha \geqslant 0} \|\tilde{\rho}^{(\alpha)} - \rho\|_2.$$

Here $\operatorname{sign}(x)$ *is* $+1$ *(resp.* -1*) if* $x > 0$ *(resp.* $x < 0$*).*

Proof. First, the α-power average converges to the max function as $p \to \infty$:

$$\lim_{\alpha \to \infty} (\tilde{\rho}^{(\alpha)})_{i,j,k} = (\tilde{\rho}^{(\infty)})_{i,j,k} := \max_{\|(i',j',k')-(i,j,k)\|_1 = 1} \rho_{i',j',k'}.$$

The logarithmic derivative of $\tilde{\rho}^{(\alpha)}$ is

$$\begin{aligned} \frac{\mathrm{d}}{\mathrm{d}\alpha} \log \tilde{\rho}^{(\alpha)} &= \frac{\mathrm{d}}{\mathrm{d}\alpha} \frac{1}{\alpha} \log \left(\frac{1}{6} \sum_{\|(i',j',k')-(i,j,k)\|_1 = 1} \rho^{\alpha}_{i',j',k'} \right) \\ &= -\frac{1}{\alpha^2} \log \left(\frac{1}{6} \sum_{\|(i',j',k')-(i,j,k)\|_1 = 1} \rho^{\alpha}_{i',j',k'} \right) + \frac{1}{\alpha} \frac{\sum_{\|(i',j',k')-(i,j,k)\|_1 = 1} \rho^{\alpha}_{i',j',k'} \log \rho_{i',j',k'}}{\sum_{\|(i',j',k')-(i,j,k)\|_1 = 1} \rho^{\alpha}_{i',j',k'}} \end{aligned}$$

and by Jensen's inequality applied to the convex function $f(x) = x \log x$ with $x = \rho^{\alpha}_{i',j',k'}$, we have

$$\frac{1}{6} \sum_{(i',j',k')} \rho^{\alpha}_{i',j',k'} \log \rho^{\alpha}_{i',j',k'} \geqslant \left(\frac{1}{6} \sum_{(i',j',k')} \rho^{\alpha}_{i',j',k'} \right) \log \left(\frac{1}{6} \sum_{(i',j',k')} \rho^{\alpha}_{i',j',k'} \right).$$

Hence the function $\alpha \mapsto \log \tilde{\rho}^{(\alpha)}$ is increasing, as is $\alpha \mapsto \tilde{\rho}^{(\alpha)}$.

Since $\alpha \mapsto \tilde{\rho}^{(\alpha)}_{i,j,k}$ is increasing, $\alpha \mapsto |\tilde{\rho}^{(\alpha)}_{i,j,k} - \rho_{i,j,k}|^2$ has two possible behaviors: increases for large α when $\tilde{\rho}^{\infty}_{i,j,k} < \rho_{i,j,k}$, or decreases for large α when $\tilde{\rho}_{i,j,k} \leqslant \rho_{i,j,k}$. The derivative of L^2-error $\|\tilde{\rho}^{(\alpha)} - \rho\|_2$ is

$$\frac{\mathrm{d}}{\mathrm{d}\alpha} \|\tilde{\rho}^{(\alpha)} - \rho\|_2^2 = \frac{1}{\alpha^2} \sum_{(i,j,k)} \operatorname{sign}(\rho_{i,j,k} - \tilde{\rho}^{\infty}_{i,j,k}) \cdot \left(\frac{1}{6} \sum_{(i',j',k')} \rho^{\alpha}_{i',j',k'} \log \rho^{\alpha}_{i',j',k'} - \log \left(\frac{1}{6} \sum_{(i',j',k')} \rho^{\alpha}_{i',j',k'} \right) \right)^2$$

and the conclusion follows. □

We found that the error function eventually increases for all of our webs, and this is a typical case in the following sense. The term after sign inside the summation in (2) is nonnegative by Jensen's inequality. Also, $\operatorname{sign}(\rho_{i,j,k} - \tilde{\rho}^{\infty}_{i,j,k}) = -1$ when $\rho_{i,j,k} < \tilde{\rho}^{\infty}_{i,j,k}$, i.e. the silk density attains local maximum at (i,j,k). In this case, all the neighboring indices (i',j',k') with $\|(i,j,k)-(i',j',k')\|_1 = 1$ satisfy $\rho_{i',j',k'} \geqslant \tilde{\rho}^{\infty}_{i',j',k'}$ and the corresponding signs are plus. In other words, most of the signs in the summation are $+1$, and this explains why the condition (2) is met.

Tables

The complete table of entropy data is provided below. "Imm." indicates immature spiders. If no sex is listed, it means the spider was too young to be sexed.

Date of Scan	Species	H in bits	H (Excl. Level 0) in bits
October 4	N. digna Female	0.07872	0.7321
October 6	N. digna Imm. male	0.08592	1.2152
October 8	N. digna Female	0.05160	0.3962
October 8	N. digna Female	0.03939	0.6771
October 17	N. digna Female	0.1691	1.3843
October 17	N. digna Female	0.1267	0.8343
October 19	N. digna Female	0.07764	1.0561
October 20	N. digna Female	0.09543	0.9638
October 26	N. digna Female	0.06353	1.3831
October 30	N. litigiosa Female	0.04780	1.2605
October 31	N. digna Male	0.06168	0.7365
November 2	N. digna Female	0.03338	1.0041
November 2	N. digna Imm. male	0.1028	1.6466
November 5	N. digna Female	0.1013	1.1862
November 7	M. dana Female	0.06297	1.1417
November 8	N. digna Female	0.06524	1.1358
November 9	M. dana Female	0.04904	1.5135
November 12	M. dana Female	0.08684	1.2542
November 12	M. dana Female	0.1085	1.8817
November 12	N. digna Female	0.04782	1.2572
November 14	N. litigiosa Female	0.08240	1.4815
November 14	M. dana Female	0.08046	1.1975
November 14	M. dana Female	0.05560	1.1184
November 14	N. digna Penultimate Male	0.08982	1.2412
November 16	N. digna Female	0.08157	1.1021
November 16	M. dana Female	0.0740	1.1154
November 17	M. dana Female	0.09874	1.3573
November 19	M. dana Imm. Male	0.03683	0.5589
November 21	N. litigiosa Female	0.05804	1.3176
November 25	M. dana Female	0.1147	1.1582
November 25	M. dana Imm. Male	0.08797	1.4670
November 25	N. digna Imm. Male	0.04294	1.4693
November 28	N. digna Female	0.06541	1.2420
November 28	N. digna Imm. Male	0.06555	1.1231
November 29	M. dana Imm. Male	0.1445	1.8521
December 1	M. dana Imm. Female	0.1295	1.5872
December 1	N. digna Female	0.07163	1.03453
December 1	N. digna Imm. Female	0.09759	1.3856
December 1	N. litigiosa Female	0.1080	1.6531
December 2	N. digna Imm. Male	0.05569	1.1196
December 4	N. digna Imm.	0.07527	1.3714
December 5	M. dana Imm. Male	0.1263	1.3638

December 5	M. dana Imm.	0.1226	0.8912
December 5	N. digna Imm. Male	0.09717	1.3576
December 5	M. dana Imm. Male	0.1227	1.5067
December 5	M. dana Imm. Female	0.05392	1.2364
December 9	M. dana Imm. Female	0.05151	1.1792
December 10	N. digna Male	0.06765	1.3831

Table 3: Entropy values for each web sample. We use 10 quantization levels for calculating the entropy.

The following Figure 5 shows the distribution of entropy data.

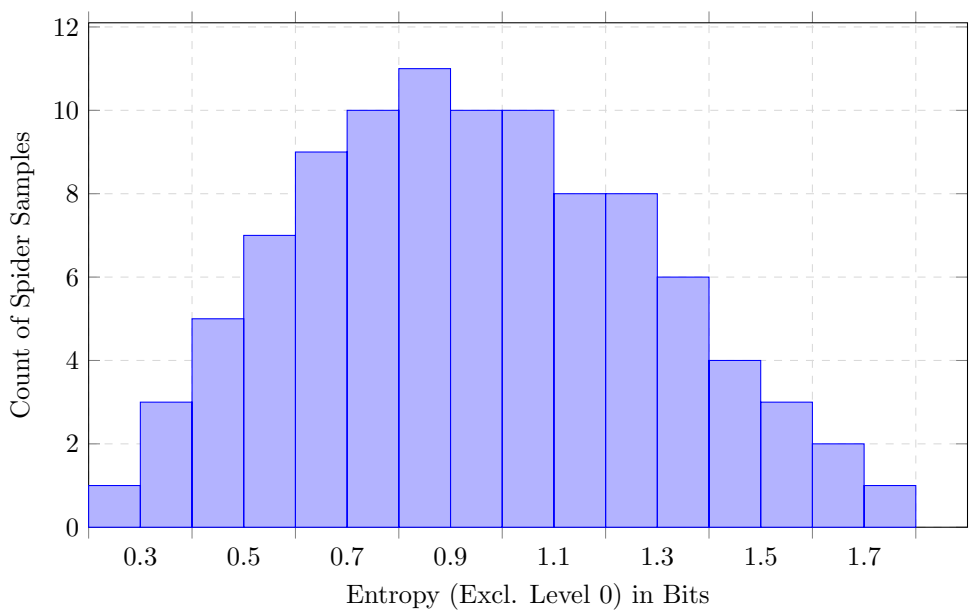

Figure 5: Histogram of Entropy Values Excluding zero-density-level using 10 density levels.

The full table of harmonicity data is as follows.

Date of Scan	**Species**	$\|\Delta\|_2$	α_*
October 4	N. digna Female	0.0073	0.81
October 8	N. digna Imm. male	0.0032	1.0
October 8	N. digna Female	0.0007	0.99
October 17	N. digna Female	0.0024	0.98
October 17	N. digna Female	0.0099	0.98
October 19	N. digna Female	0.0027	1.02
October 20	N. digna Female	0.0023	0.98
October 26	N. digna Female	0.0019	0.96

October 30	To be filled in	0.0026	0.97
October 31	N. digna Female	0.0049	1.0
November 2	N. litigiosa Female	0.0027	0.97
November 5	N. digna Female	0.0011	0.93
November 7	N. digna Imm. male	0.0095	0.97
November 8	N. digna Female	0.0032	0.81
November 9	N. digna Female	0.0074	0.92
November 12	M. dana Female	0.0018	0.97
November 12	N. digna Female	0.0033	0.89
November 12	Therrid spp.	0.0018	0.86
November 14	M. dana Female	0.0034	0.91
November 14	M. dana Female	0.0051	0.95
November 14	M. dana Female	0.0067	0.97
November 14	N. digna Female	0.0042	1.0
November 14	N. litigiosa Female	0.0042	0.92
November 14	M. dana Female	0.0034	0.96
November 14	M. dana Female	0.0032	0.96
November 14	N. digna Penultimate Male	0.0070	0.95
November 16	N. digna Female	0.0036	0.96
November 16	M. dana Female	0.0053	0.96
November 17	M. dana Female	0.0052	1.0
November 19	M. dana Imm. male	0.0018	0.85
November 21	N. litigiosa Female	0.0024	0.96
November 25	M. dana Female	0.0059	0.89
November 25	M. dana Imm. Male	0.0040	0.88
November 25	N. digna Imm. Male	0.0021	1.0
November 28	N. digna Female	0.0049	1.02
November 28	N. digna Imm. Male	0.0026	0.91
November 29	M. dana Imm. Male	0.0076	0.98
December 1	M. dana Imm. Female	0.0018	0.97
December 1	N. digna Female	0.0034	0.91
December 1	N. digna Imm. Female	0.0051	0.95
December 1	N. litigiosa Female	0.0067	0.97
December 2	N. digna Imm. Male	0.0042	1.0
December 4	N. digna Imm.	0.0053	0.96
December 5	M. dana Imm. Male	0.0052	1.0
December 5	M. dana Imm.	0.0018	0.85
December 5	N. digna Imm. Male	0.0024	0.96
December 5	M. dana Imm. Male	0.0059	0.89
December 5	M. dana Imm. Female	0.0040	0.88
December 9	M. dana Imm. Female	0.0021	1.0
December 10	N. digna Male	0.0049	1.02

Table 4: 2-norm of the Laplacian for each web sample. We use 20 subdivisions on the length and width dimensions and 15 subdivision on the height dimension.